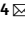# scientific **data**

Check for updates

OPEN

DATA DESCRIPTOR

Age-specific ASPECTS atlas of Chinese subjects across different age groups for assessing acute ischemic stroke

Qi Sun[1,2,6], Guan Wang[3,6], Jinzhu Yang [1,2,4 ✉], Yimo Zhou[3], Yuliang Yuan[1,2], Yan Huang[1,2] & Ziyu Fu[5]

The Alberta Stroke Program Early Computed Tomography Score (ASPECTS) is a valuable and easy-to-use method for assessing acute ischemic stroke. It aids in identifying suitable candidates for thrombolytic therapies and evaluating treatment effectiveness. However, ASPECTS evaluation primarily relies on visual observation in current clinical practice, lacking a common standardized space. Additionally, different doctors may have varying clinical experiences, leading to a poor inter-reader agreement and potential errors in the final ASPECTS scoring. To address these issues and fill in the absence of a publicly available ASPECTS atlas, this work constructs age-specific Chinese ASPECTS atlases based on non-contrast computed tomography images of 281 healthy subjects across different age groups. Images of different age groups are warped into respective common averaged spaces, where the average intensity atlases are computed. More importantly, 10 ASPECTS regions can be obtained during this process. We develop an automated ASPECTS region mapping pipeline and collect an independent dataset to validate our atlas. The results prove that the age-specific ASPECTS atlas is of great promise in clinical availability.

Background & Summary

Stroke is the second leading cause of death worldwide and is characterized by high incidence, high recurrence rate, high disability rate, high mortality rate, and high economic burden. More than 13.7 million people are affected by this disease, and about 5.8 million people die as a result each year[1,2]. Particularly in China, stroke has become the leading cause of death and disability in adults, with a lifetime risk of 39.9%, ranking first globally and showing a trend of affecting younger individuals[3]. However, due to limited medical resources, the timely treatment rate for stroke patients in China is only 2%, resulting in over 2 million deaths and a disability rate of up to 80% each year[4]. According to the worldwide stroke incidence, ischemic stroke accounts for over 70% of all stroke cases[5]. Research has shown that completing basic assessments such as brain non-contrast computed tomography (NCCT) within 60 minutes of acute ischemic stroke (AIS) onset, administering thrombolytic therapy within 4.5 hours, and performing mechanical thrombectomy within 6 hours (up to 24 hours) to restore blood flow and recanalize vessels can significantly reduce the disability and mortality rates associated with stroke[6]. Therefore, rapid and accurate assessment of AIS is of great significance for improving patients' quality of life and prognosis.

In clinical practice, NCCT and magnetic resonance imaging (MRI) are two important imaging examination methods for the diagnosis of AIS[6,7]. Diffusion weighted imaging (DWI) and fluid attenuated inversion recovery (FLAIR) images are considered the gold standards for AIS imaging diagnosis due to their high resolution and lesion sensitivity. However, the longer scan time and higher cost limit their widespread use, especially in remote areas and grassroots hospitals. In comparison, NCCT has the advantages of wide availability and low cost. It can

[1]Key Laboratory of Intelligent Computing in Medical Image, Ministry of Education, Northeastern University, Shenyang, Liaoning, China. [2]School of Computer Science and Engineering, Northeastern University, Shenyang, Liaoning, China. [3]Department of Radiology, The First Hospital of China Medical University, Shenyang, Liaoning, China. [4]National Frontiers Science Center for Industrial Intelligence and Systems Optimization, Shenyang, Liaoning, China. [5]Institute of Pure and Applied Sciences, University of Tsukuba, Tsukuba, Japan. [6]These authors contributed equally: Qi Sun, Guan Wang. ✉e-mail: yangjinzhu@cse.neu.edu.cn

quickly assess the brain condition of patients within a short period and has reliable sensitivity and specificity for AIS. The Alberta Stroke Program Early Computed Tomography Score (ASPECTS) is a simple and reliable systematic method that can effectively evaluate early ischemic changes in the blood supply region of the middle cerebral artery (MCA) on NCCT semi-quantitatively. It provides reliable clinical evidence for selecting thrombolytic drugs, treatment plan formulation, assessment of thrombolysis efficacy, and long-term prognosis[7–9]. In ASPECTS, the MCA vascular territory is divided into 10 regions in each hemisphere, with M1 corresponding to the frontal operculum, M2 to the anterior temporal lobe, M3 to the posterior temporal lobe, M4 to the anterior superior frontal cortex, M5 to the posterior frontal cortex, and M6 to the parietal cortex. The M4, M5, and M6 are the MCA territories superior to the M1, M2, and M3 regions, respectively. The four subcortical regions include caudate (C), lentiform (L), internal capsule (IC), and insular (I)[8]. If any region shows signs of ischemic change, 1 point is deducted from the initial score of 10 points[10]. Clinical results indicate that patients with ASPECTS > 6 are suitable for intravascular thrombectomy[7]. However, several factors hinder the clinical application of ASPECTS. On the one hand, manually annotating the 10 ASPECTS regions is time-consuming. On the other hand, physicians with different clinical experiences may achieve poor inter-reader agreement, which significantly affects the formulation of subsequent treatment plans. Therefore, there is an urgent need for a standardized NCCT atlas to improve the agreement of ASPECTS evaluation, enhance diagnostic efficiency, and reduce the reliance on individual expertise.

Many well-known brain atlases have been developed for neuroimaging research and clinical purposes. To begin with, the non-digital Talairach atlas, which was developed based on the brain anatomy of a 60-year-old female, played an important role in the early study of brain function. Later, the Montreal Neurological Institute (MNI) created the widely used MNI305 atlas[11,12] by non-linearly registering 305 brain MRI images into a common space. Because of the blurriness of the MNI305, the ICBM152[13–15] was then constructed using higher-resolution MRI images of 152 normal Caucasian individuals. Compared with these average intensity atlases, the cortical structure probabilistic brain atlas, LPBA40[16], was generated using T1-weighted MRI images of 40 healthy individuals with an average age of 29.2 years. It includes annotation for 50 cortical structures, 4 subcortical regions, the brainstem, and cerebellum. For the Chinese population, the Chinese56 atlas[17] was developed based on 56 Chinese males with an average age of 24.46 years and demonstrated significant differences between the Caucasian and Chinese brain atlases through morphological measurements. To explore differences in brain structure across different age groups, the Chinese2020 atlas[18] was constructed based on a multi-center high MRI dataset of 2020 Chinese adults. It contains 12 atlases from the age 20 year to the age 75 year at a 5 years interval and is also proved to be more suitable for the Chinese population.

The above MRI-based atlases can provide clear brain structure information, but they cannot be used to analyze images from other modalities due to the impact of imaging modality differences on registration accuracy. To meet more clinical needs, a stroke-control CT (scCT) atlas[19] was developed, based on 30 healthy individuals with an average age of 61.3 years, to assist in diagnosing stroke in the elderly. Similarly, a high-resolution 3D NCCT brain atlas[20] using 47 NCCT scans with an average age of 72 years was also created. Although these atlases can address the registration accuracy issue caused by modality differences, they still have certain limitations for the clinical utility of ASPECTS. On the one hand, these atlases are limited regarding the age distribution. The age-related brain changes (*e. g.*, atrophy of gray and white matter) may affect the spatial correspondences between patient images and the atlas. On the other hand, the lack of ASPECTS region information makes it challenging to perform a rapid and accurate diagnosis of AIS.

To fill in the absence of an available ASPECTS atlas and remedy the limitations of existing atlases, this work constructs the Chinese ASPECTS atlas based on 281 brain NCCT images of healthy subjects across four age groups: 10-29 years, 30-49 years, 50-69 years, and 70-89 years. The proposed atlas, referred to as the ASPECTS-281 atlas, contains average intensity images and the corresponding ASPECTS regions. The age-specificity improves the generalization and robustness of the atlas, and consequently its utility. ASPECTS-281 is the first publicly-available, digital ASPECTS atlas that can be readily used in neuroscience and clinical practice, assisting in achieving rapid and highly reproducible ASPECTS scoring.

Methods

Datasets. A retrospective analysis was conducted on brain NCCT images of individuals who participated in the comprehensive health screening program at the First Hospital of China Medical University from November 2021 to June 2023. Based on the differences in brain anatomical structure across different age groups, the individuals were divided into four age groups: 10-29 years, 30-49 years, 50-69 years, and 70-89 years, with each group comprising 66, 75, 87, and 53 subjects, respectively. The average ages of these four groups were 19.9 ± 5.0 years, 40.0 ± 5.6 years, 58.2 ± 5.7 years, and 76.9 ± 5.6 years (mean $\pm$ standard deviation). Overall, the proportion of male subjects was higher than female. Exclusion criteria included significant deviation of the scan baseline from the orbitomeatal line (OML), a history of neurological or psychiatric disorders, as well as major intracranial findings detected on CT scans, such as intracranial hemorrhage, infarction, ischemia, and masses. These images were obtained using 15 different scanners (Brilliance 64, Optima CT680 Series, SOMATOM Definition Flash, NeuViz Epoch, uCT 760, SOMATOM Definition, Discovery CT750 HD, SOMATOM Force, uCT 960, NeuViz Glory, NeuViz Prime, Revolution CT, SOMATOM Drive, iCT 256, Aquilion ONE) from 6 manufacturers (GE MEDICAL SYSTEMS, UIH, NMS, SIEMENS, Philips, and Toshiba). The scan range extended from the base of the posterior fossa to the vertex, with a uniform image resolution of 512×512 and a slice thickness of 5 *mm*. The pixel size ranged from 0.39 to 0.57 *mm*, and the tube voltage was 120 kV.

Besides, we collected an independent validation set consisting of brain NCCT images of 91 subjects, with 23, 20, 24, and 24 subjects in the respective age groups. This dataset was acquired between January 2023 and January 2024 from the First Hospital of China Medical University. There was no subject overlap between the validation set and the construction set. The images were obtained using multiple CT scanners (Optima CT680 Series,
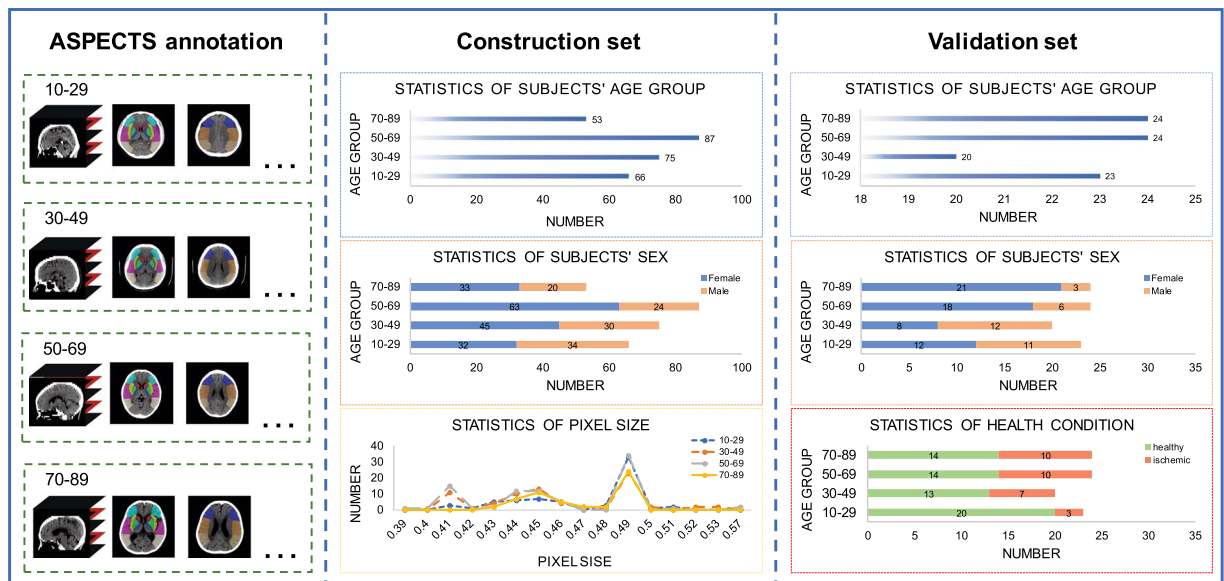
Fig. 1 Detailed statistics of the construction and validation sets of the ASPECTS-281.

Discovery CT750 HD, uCT 960, NeuViz Epoch, SOMATOM Force, and SOMATOM Drive) with a tube voltage of 120 kV. The scan range, slice thickness, and image resolution matched those of the construction set. Our ultimate aim is to provide a pipeline that can be applied to clinical populations with ischemic stroke. Therefore, we intentionally included a certain number of ischemic subjects, who all underwent NCCT scans within 12 hours of symptom onset, and there were areas of low intensity ischemic lesions in the MCA regions.

A waiver of consent for this study was approved by the Northeast University Biological and Medical Ethics Committee (Ethics Review Number: NEU-EC-2023B034S). All the data used in this study comes from previous clinical diagnoses and treatments, with the risks to subjects not exceeding minimal risk (minimal risk refers to the likelihood and severity of expected risks in the study being no greater than those encountered in daily life or during routine physical examinations or psychological tests). The waiver of consent will not adversely affect the rights and health of the subjects. Additionally, we have fully anonymized the data, which does not contain any personal privacy information (such as patient name, ID, date of birth, or other sensitive information) and does not use medical records or data that subjects have explicitly refused to allow. This study also does not involve any commercial interests. Detailed statistics of both datasets are presented in Fig. 1.

Pre-processing. The main purposes of the pre-processing were to generate ASPECTS region annotation and standardize all NCCT images. According to the definition of ASPECTS, two key CT axial slices needed to be pre-determined: one at the level of the thalamus and basal ganglia, and another just rostral to the ganglionic structures[8] (In the following text, we use the basal ganglia level (BGL) and supraganglionic level (SGL) to represent these two slices, respectively[21,22]). This work was completed by a neurologist (G.W.) with over 10 years of clinical experience in neuroscience. Meanwhile, 10 ASPECTS regions corresponding to the middle cerebral vascular territories[23] were manually annotated on these two slices of each subject as the ground truth (C=1, L=2, IC=3, I=4, M1-M6=5-10). For the validation set, two other neuroradiologists, namely Rater-1 and Rater-2, with 5 and 4 years of relevant clinical experience, were asked to independently annotate the ASPECTS regions on the pre-defined BGLs and SGLs. Their annotations were used as comparative references to evaluate the agreement of ASPECTS region mapping. In the annotation procedure, we excluded the sulcus in subjects aged 70-89 years since these regions were remarkable in this age group. To accelerate the following process of atlas construction, we pre-aligned the mid-sagittal plane to be in the vertical center of the image space. For a horizontally symmetric brain CT image X, it should have the minimum difference from its horizontally flipped version X'. Based on this premise, we employed the alignment sub-network T of the Symmetry-Enhanced Attention Network[24] to accomplish the task. The alignment network T is an unsupervised 3D transformation network that uses the $L1$ loss of X and X' as the loss function. Its output parameters $\alpha \in \mathbb{R}^6$ include translation $\alpha_{1:3}$ and rotation $\alpha_{4:6}$ components of the x, y, and z axes. Since we considered the horizontal symmetry of the image, only the translation in the x-direction and rotation along the z-axis were used to generate the quasi-symmetric image $X' = T(X)$ based on a parameterized sampling grid[25]. The final transformation was applied to the raw NCCT images and ASPECTS regions.

Furthermore, we performed threshold-based and region-based brain tissue extraction on these two slices to eliminate the skull and other non-brain tissue. Specifically, a confidence-based growing algorithm was first used to produce a coarse brain mask, where the threshold range was set to 0-120 Hounsfield Unit (HU), the initial neighborhood radius was set to 5 pixels, and the standard deviation multiplier was set to 12. The morphology-based method was then used to recover tissue with low intensity that had been mistakenly removed to ensure the integrity of all brain masks (radius=10 pixels). Finally, the largest connected region was extracted in the image as the final brain mask. All processed brain masks underwent visual inspection by the neurologist
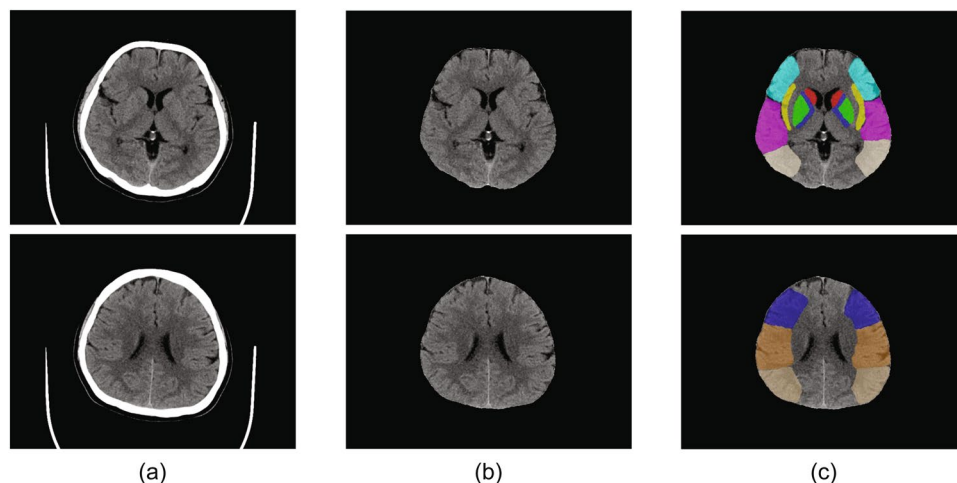
Fig. 2 Example of the pre-processing result. (**a**) Raw NCCT image. (**b**) Result of the image alignment and brain tissue extraction. (**c**) Manual annotations of 10 ASPECTS regions.
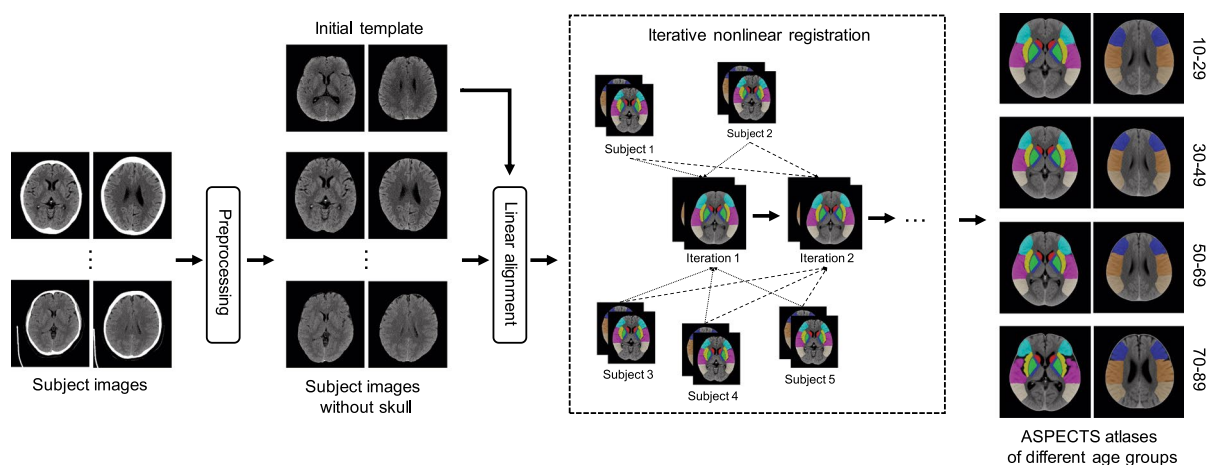

Fig. 3 Construction pipeline of the ASPECTS-281 atlas.

(G.W.) to identify extraction errors, and were manually corrected if necessary. We did not perform intensity normalization but normalized the in-plane resolution to $0.5 \times 0.5 \, mm^2$ for all subjects using linear interpolation. One example of the pre-processing results along with its corresponding ASPECTS region annotation is shown in Fig. 2.

Atlas construction.   The overall construction pipeline of the ASPECTS-281 atlas is shown in Fig. 3. After the pre-processing, an initial template was randomly selected from images of each age group. Then affine registration (rotation, translation, scaling) was performed to spatially align all images within the age group to the initial template. Finally, a symmetric diffeomorphic elastic registration algorithm[26] based on cross-correlation similarity metric was applied to achieve the non-linear deformations. As the iterations increased, the images gradually converged toward the spatial geometric center, ultimately producing the average intensity atlas. We utilized the workflow defined in the *antsMultivariateTemplateConstruction*2.*sh* script from the Advanced Normalization Tools (ANTs, http://stnava.github.io/ANTs/)[27]. Default parameters were adopted to construct the atlas, including the iteration number (default=4), sharpening applied to the template at each iteration (default = Laplacian), similarity metric used for pairwise registration (default = CC), and transformation model used for registration (default = SyN). We tested other similarity metrics for the registration, such as mutual information (MI), mean square difference (MSD), and other non-linear registration schemes to improve the quality of the atlas. However, by visual inspection, we found that the default option of this script yielded the best results. Additionally, we evaluated the atlases generated with different numbers of iterations, and the corresponding visualization results of deformation fields are shown in Fig. 4. As the number of iterations increases, the deformation field gradually flattens out, indicating that the differences between warped subjects and each intermediate atlas gradually decrease. To strike a balance between the quality of the atlas and the efficiency of the construction process, we set the numberof iterations to 4.
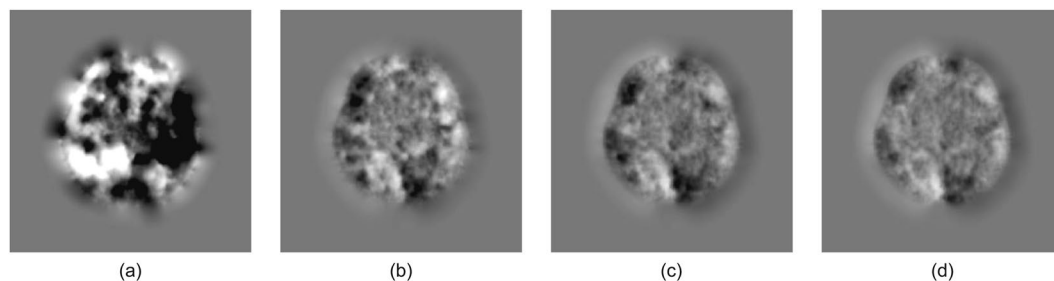
Fig. 4 Evolution in deformation fields during the atlas construction process. The figures from (**a**–**d**) correspond to the deformation fields of the iteration 1 to 4. The high and low intensity represents positive and negative deformation, respectively.
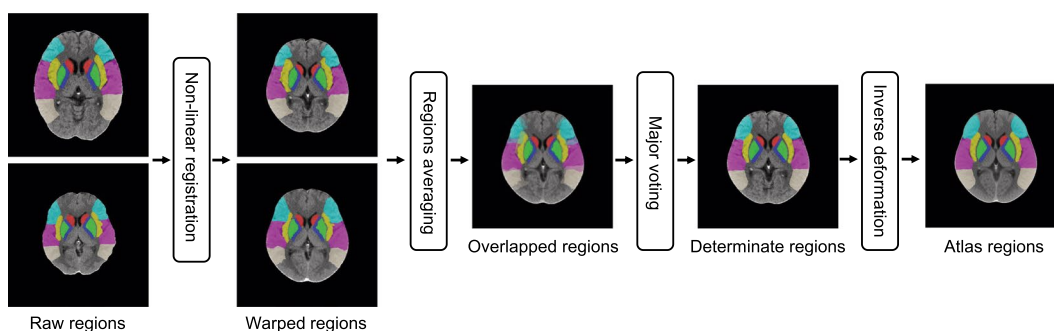

Fig. 5 Deformation process of the ASPECTS regions.

ASPECTS		
Age group	SGL	BGL
10-29	SGL_image_10_29.nii.gz / SGL_label_10_29.nii.gz	BGL_image_10_29.nii.gz / BGL_label_10_29.nii.gz
30-49	SGL_image_30_49.nii.gz / SGL_label_30_49.nii.gz	BGL_image_30_49.nii.gz / BGL_label_30_49.nii.gz
50-69	SGL_image_50_69.nii.gz / SGL_label_50_69.nii.gz	BGL_image_50_69.nii.gz / BGL_label_50_69.nii.gz
70-89	SGL_image_70_89.nii.gz / SGL_label_70_89.nii.gz	BGL_image_70_89.nii.gz / BGL_label_70_89.nii.gz

Table 1. File list of the ASPECTS-281 atlas.

Compared with other atlas construction processes, we also utilized the obtained linear and non-linear deformation fields to generate the warped ASPECTS regions. To achieve this goal, the affine matrices, deformation fields, and inverse deformation fields produced during the registration process were saved, where the two fields contained the non-linear deformation from the warped subjects to the intermediate atlas, and the corresponding inverse non-linear deformation, respectively. We first calculated the average ASPECTS regions based on the affine matrices and deformation fields. Since each region strictly corresponds to a binary label, we used majority voting to determine the identification of the current region when different regions overlapped with one another. Then, we calculated the average inverse deformation and used it to generate the final warped ASPECTS regions. The whole process of region deformation is shown in Fig. 5. The constructed average intensity atlases and the corresponding ASPECTS regions were reviewed and confirmed by the neurologist (G.W.).

Data Records
The constructed ASPECTS-281 atlas is available at figshare[28] (https://doi.org/10.6084/m9.figshare.26819290). Atlas files are divided into two categories, one corresponding to the BGL and the other to the SGL, and are stored in the NIfTI format with an in-plane resolution of $0.5 \times 0.5\,mm^2$. The detailed file list is summarized in Table 1. The suffix of each file name identifies the specific age group. Files with the keyword *image* are the average intensity atlases, stored in short precision, while files with the keyword *label* are the corresponding ASPECTS region atlases, stored in unsigned char format.

Technical Validation
The ASPECTS atlas. Figure 6 shows the final average intensity atlases and the corresponding ASPECTS regions across four age groups. The former serves as a standardized template for spatial normalization of brain NCCT images, while the latter provides ASPECTS regions for the subsequent diagnostic and treatment plans. The ASPECTS-281 atlas not only accurately reflect the general morphology of relevant anatomical structures, but also
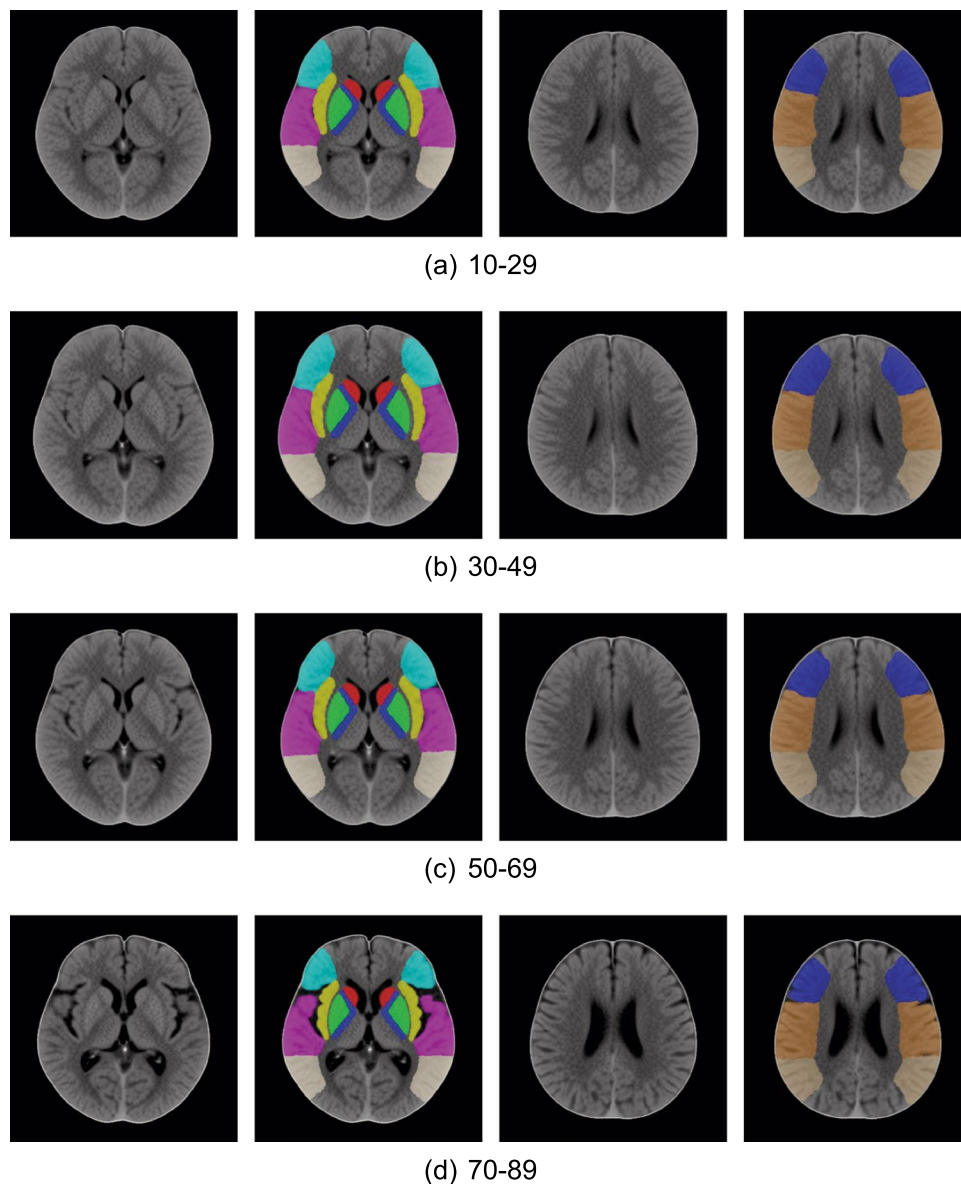
(a) 10-29

(b) 30-49

(c) 50-69

(d) 70-89

Fig. 6 Constructed age-specific ASPECTS-281 atlas. The atlas for each age group includes an average intensity atlas and the corresponding ASPECTS regions.

enhance the accuracy of ASPECTS region mapping in clinical practice. We evaluated the constructed atlas from two aspects: image quality and the accuracy of ASPECTS region mapping. The paired T-test was used to assess the differences in the following comparison results, with a p-value less than 0.05 indicating a significant difference.

Atlas quality validation. The image quality of our ASPECTS-281 was validated from both visual inspection and quantitative analysis perspectives. As shown in Fig. 6, the boundaries of the critical nuclei, as well as the gyri and sulci, are sharp and clear. Additionally, the boundaries of the brain exhibit excellent smoothness. By comparing the atlases of different age groups, noticeable changes in relevant anatomical structures of the brain can be observed. As age increases, the sulci are more pronounced due to the atrophy of gray and white matter, which is particularly remarkable after the age of 70 years. This is consistent with the actual morphological changes in brain tissue. In terms of quantitative analysis, we introduced the image entropy, which is a quantitative metric to assess the sharpness of an image[29]. The lower the entropy, the sharper the image. The image entropy is defined as follows:

$$E(X) = -\sum(p(x)\log_2(p(x)))$$

(1)

where $p(x)$ is the probability of each intensity level. To calculate the image entropy, each atlas was first normalized to 0-255. Then, the probability histogram was computed, where each bin represents the ratio of the occurrence frequency of an intensity value to the sum of the occurrence frequencies of all 256 intensity values. Table 2 summarizes the entropies of our average intensity atlases of different age groups in comparison with the

Atlas	Age group	Age (mean ± std)	Subject number	Entropy (BGL / SGL / Mean)
ASPECTS-281	10-29	19.9 ± 5.0	66	2.22 / 2.09 / 2.15
	30-49	40.0 ± 5.6	75	2.37 / 2.09 / 2.23
	50-69	58.2 ± 5.7	87	2.30 / 2.15 / 2.23
	70-89	76.9 ± 5.6	53	2.24 / 2.11 / 2.18
MIPLAB-NCCT	—	71.9 ± 14.0	47	2.80 / 2.45 / 2.63
scCT	—	61.3 ± 18.4	30	3.65 / 3.31 / 3.48

Table 2. Entropy of the ASPECTS-281 in comparison with the MIPLAB-NCCT atlas and scCT atlas.
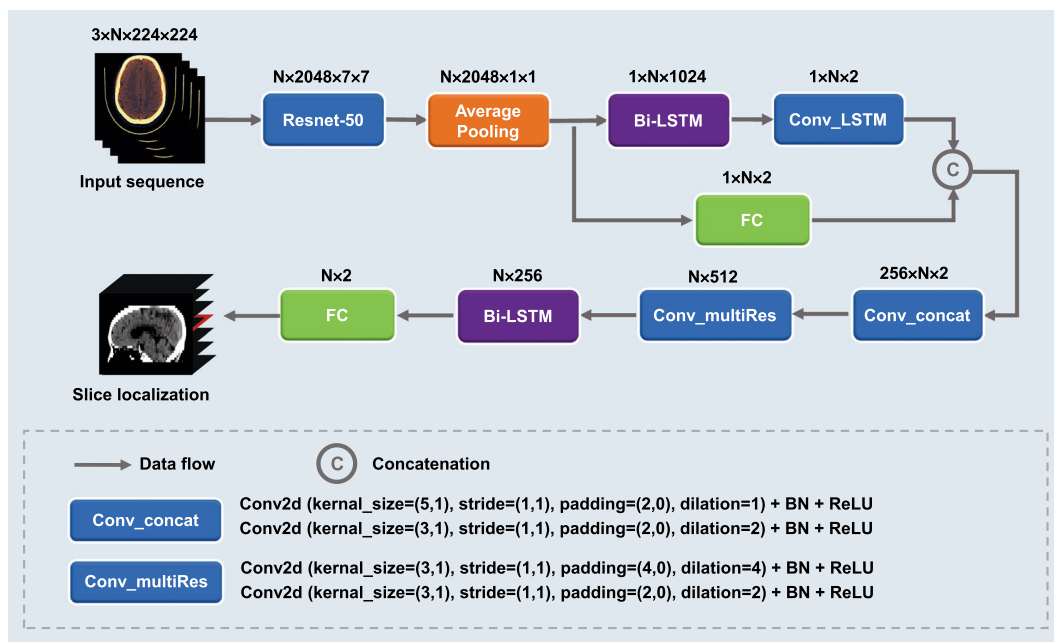

Fig. 7 Architecture of the ASPECTSLoc-Net. The number annotated on each module represents the dimension of the output features of the current layer, and N corresponds the slice number of the brain NCCT image.

MIPLAB-NCCT atlas[20] and scCT atlas[19]. Since both of these atlases are 3D atlases, we selected the corresponding slices for the BGL and SGL to calculate the image entropy. Brain tissue extraction was performed on the scCT atlas to remove the non-brain tissue. It can be observed that our ASPECTS-281 atlas exhibits lower entropy (i.e., better detail and sharpness) and shows a significant difference compared with the other two atlases ($p < 0.05$).

ASPECTS region validation. To validate our atlas and enhance its clinical utility, we developed an automated pipeline that encompassed specific ASPECTS slices localization, brain tissue extraction, spatial normalization, and ASPECTS region mapping. The ASPECTS slice localization aims to automatically identify the BGL and SGL from a brain NCCT image. To achieve this, we devised a deep neural network called ASPECTSLoc-Net, as illustrated in Fig. 7.

ASPECTSLoc-Net processes a sequence of 2D axial brain NCCT slices and outputs the slice index of the BGL. A 2D ImageNet-pretrained ResNet-50 without the fully connected (FC) layer is employed as the encoder to extract features from different slices, generating 2048 features for each input slice. Subsequently, a bi-directional long short-term memory (Bi-LSTM)[30] layer with 512 hidden units is introduced to capture the relationships among neighboring slices. To further aggregate inter-slice features, we concatenate the pre-classification results and the output features of the first Bi-LSTM and pass them through two consecutive multi-resolution feature extraction layers. Finally, another Bi-LSTM layer is employed to locate the BGL. After the localization of the BGL, it is then used as a reference to determine the SGL (Clinically, it is generally believed that the SGL is 2 cm above the BGL). The input of the network is an RGB-like image obtained by stacking three instances from different windows commonly used in brain CT diagnosis: brain window (WL=40, WW=80), subdural window (WL=75, WW=215), and bony window (WL=600, WW=2800), where WL and WW represent window level and window width, respectively. Input images are all linearly pre-downsampled to 224 × 224.

All experiments were implemented by PyTorch 1.7.1 with an NVIDIA A30 with 24 GB of memory on Ubuntu 18.04.6 LTS system. We used the binary cross entropy as the loss function. ASPECTSLoc-Net was trained for 100 epochs using the Adam optimizer with an initial learning rate of 0.001 and a cosine annealing schedule with linear warm-up. Various augmentations, including random cropping and resizing, horizontal/vertical flip, random rotation between 0° and 30°, grid distortion, Gaussian noise, and CutMix[31] with $\alpha = 1$, were
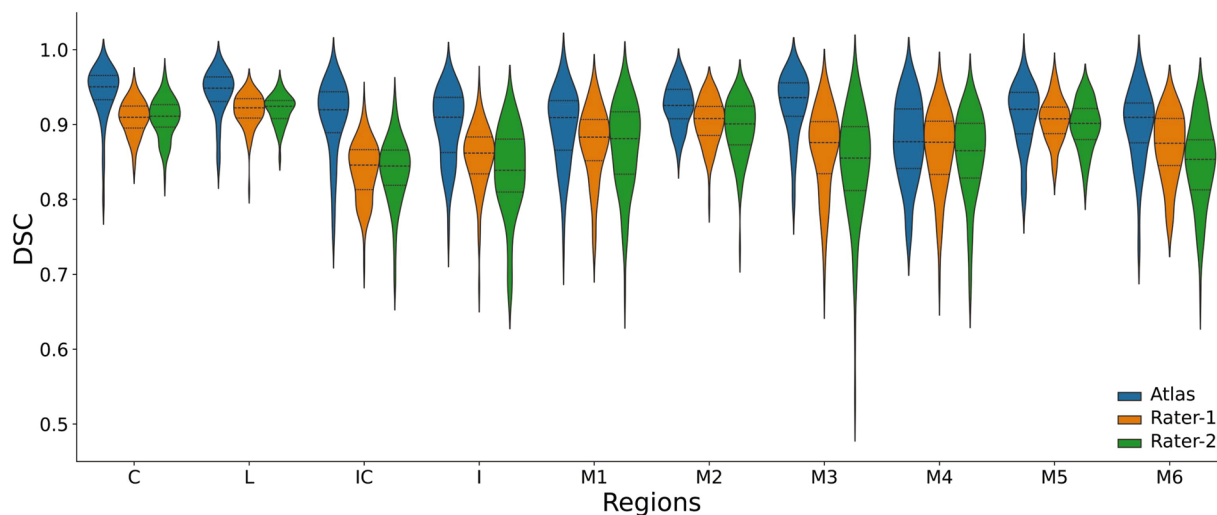
Fig. 8 DSC for ASPECTS region mapping of the validation set. The dashed line and the two dotted lines in each violin plot represent the median and the upper/lower quartile boundaries, respectively.

ASPECTS region										
	C	L	IC	I	M1	M2	M3	M4	M5	M6
Atlas-Rater1	0.896	0.910	0.827	0.846	0.862	0.890	0.870	0.842	0.882	0.854
Atlas-Rater2	0.898	0.914	0.830	0.831	0.863	0.884	0.849	0.842	0.874	0.830
Atlas-Neurologist	0.942	0.942	0.908	0.898	0.896	0.926	0.926	0.879	0.912	0.898
Atlas Mean	0.912	0.922	0.855	0.858	0.874	0.900	0.882	0.854	0.889	0.860
Rater1-Rater2	0.898	0.914	0.822	0.819	0.855	0.885	0.835	0.836	0.881	0.836
Rater1-Neurologist	0.909	0.919	0.838	0.856	0.874	0.903	0.866	0.865	0.906	0.870
Rater2-Neurologist	0.909	0.920	0.837	0.837	0.870	0.895	0.845	0.859	0.890	0.848
Rater Mean	0.905	0.918	0.833	0.837	0.867	0.894	0.849	0.853	0.895	0.851

Table 3. DSC from the multi-GT cross-comparison between atlas-based and rater-based mapping results. Atlas-Rater1, Atlas-Rater2, and Atlas-Neurologist represent the DSC between atlas-based registration results and each GT. Rater1-Rater2, Rater1-Neurologist, and Rater2-Neurologist represent the DSC between the different raters.

applied during training. We evaluated the model's performance using the localization accuracy and inter-slice relative distance error (IS-RDE), where the IS-RDE represents the distance (in *mm*) between the predicted image slice and the ground truth (GT). Training and validation were performed using the construction set through 5-fold cross-validation. The mean localization accuracy and IS-RDE can reach 89.38% and 0.53 *mm*, respectively. Additionally, we tested the model on the validation set, achieving a localization accuracy of 82.42% and an IS-RDE of 0.88 *mm*.

After localizing the key ASPECTS slices, we performed brain tissue extraction of these two axial slices, registered the corresponding age-specific average intensity atlas to the subject's image, and mapped the 10 ASPECTS regions accordingly. The accuracy of the mapping results was measured using the Dice Similarity Coefficient (DSC):

$$DSC = \frac{2|A \cap B|}{|A| + |B|} \tag{2}$$

where A and B are two regions under comparison. DSC ranges between 0 and 1, where 1 indicates perfect matching. We conducted two experiments to evaluate the accuracy and agreement of ASPECTS region mapping. First, the annotations of the neurologist were used as the GT, while the annotations of two other raters (Rater-1 and Rater-2) served as references for comparison. We separately calculated the DSC for all ASPECTS regions of the validation set obtained by Rater-1, Rater-2, and the atlas-based registration method against the GT. The quantitative analysis results are shown in Fig. 8. The atlas-based registration method can achieve a higher DSC of 0.913 ± 0.021 (mean ± standard deviation) for 10 ASPECTS regions. In contrast, the mean DSCs are 0.880 ± 0.027 and 0.872 ± 0.031 for Rater-1 and Rater-2, respectively. It is worth noting that there is significant annotation discrepancy between Rater-1 and Rater-2 among different subjects in the insula and M1-M6 regions, with mean standard deviations of 0.044 and 0.054, respectively. This is due to the complex intensity distribution of the insula and the lack of explicit boundaries for the M1-M6 regions. For non-academic or less experienced doctors, these discrepancies may be even greater. Then, we employed a multi-GT cross-comparison method,
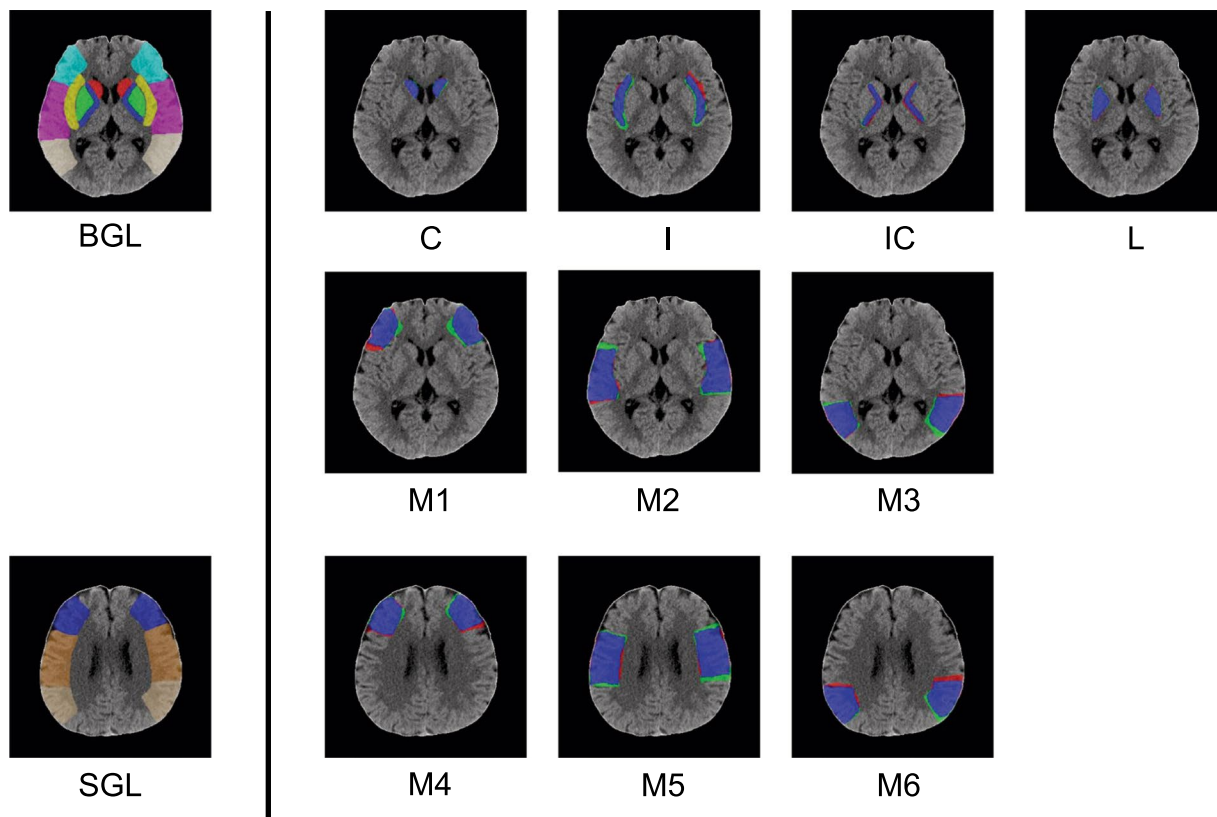
Fig. 9 Example of mapping results for 10 ASPECTS Regions. The left side shows the manually annotated ASPECTS regions (ground truth), while the right side displays the differences between the mapping results and the ground truth. In the difference map, blue indicates the overlapping area, red indicates the under-mapped area, and green indicates the over-mapped area.

ASPECTS region												
Atlas	Validation	C	L	IC	I	M1	M2	M3	M4	M5	M6	Mean
10-29	10-29	0.941	0.948	0.909	0.912	0.933	0.943	0.941	0.915	0.938	0.912	0.929
	30-49	0.926	0.933	0.885	0.886	0.879	0.906	0.847	0.842	0.906	0.852	0.886
	50-69	0.913	0.901	0.830	0.873	0.871	0.899	0.866	0.835	0.892	0.862	0.874
	70-89	0.852	0.887	0.748	0.789	0.870	0.858	0.832	0.840	0.869	0.794	0.834
30-49	10-29	0.925	0.932	0.884	0.840	0.870	0.913	0.841	0.834	0.912	0.878	0.883
	30-49	0.950	0.951	0.921	0.895	0.900	0.935	0.932	0.885	0.921	0.900	0.919
	50-69	0.931	0.923	0.870	0.835	0.846	0.909	0.913	0.842	0.894	0.885	0.885
	70-89	0.873	0.915	0.808	0.710	0.829	0.875	0.897	0.808	0.847	0.846	0.841
50-69	10-29	0.929	0.921	0.861	0.886	0.891	0.922	0.877	0.831	0.892	0.896	0.891
	30-49	0.935	0.941	0.893	0.899	0.900	0.927	0.921	0.882	0.902	0.869	0.907
	50-69	0.940	0.935	0.902	0.893	0.900	0.919	0.933	0.890	0.904	0.884	0.910
	70-89	0.899	0.931	0.865	0.780	0.855	0.881	0.896	0.807	0.827	0.819	0.856
70-89	10-29	0.884	0.897	0.753	0.854	0.846	0.871	0.829	0.888	0.913	0.855	0.859
	30-49	0.890	0.929	0.822	0.793	0.837	0.891	0.904	0.841	0.894	0.896	0.870
	50-69	0.896	0.925	0.842	0.837	0.839	0.897	0.896	0.834	0.888	0.888	0.874
	70-89	0.938	0.939	0.907	0.896	0.884	0.913	0.910	0.869	0.905	0.893	0.905

Table 4. DSCs for the ASPECTS regions using atlases of different age groups. The first column corresponds to the age groups of the atlas, and the second column corresponds to the different age groups in the validation set.

where the annotations from the neurologist, Rater-1, and Rater-2 were each considered to be GT. We calculated the DSC between the atlas-based registration mapping results and each GT, as well as the DSC between the different raters' annotations. This experiment allowed us to analyze whether the atlas-based registration method could achieve better agreement compared to manual annotations. As shown in Table 3, the mean DSC obtained

from atlas-based registration (C: 0.912, L: 0.922, IC: 0.855, I: 0.858, M1: 0.874, M2: 0.900, M3: 0.882, M4: 0.854, M5: 0.889, M6: 0.860) is higher than the mean DSC between raters (C: 0.905, L: 0.918, IC: 0.833, I: 0.837, M1: 0.867, M2: 0.894, M3: 0.849, M4: 0.853, M5: 0.895, M6: 0.851) across most ASPECTS regions ($p < 0.05$). One example of the region mapping result is presented in Fig. 9.

In addition, we analyzed the accuracy of ASPECTS region mapping separately for ischemic subjects. Due to the blurring of boundaries and attenuation anomalies caused by ischemic lesions, the mean ASPECTS region mapping accuracy for ischemic subjects is 0.882, which is lower than the 0.924 observed for healthy subjects. Furthermore, we compared the mean DSC of all ASPECTS regions obtained from different age group atlases. As shown in Table 4, using the atlas from the specific age group could yield better results with 0.929, 0.919, 0.910, and 0.905, respectively ($p < 0.01$).

In terms of efficiency, manually annotating ASPECTS regions took about 15 minutes per patient, while our fully automated pipeline completed the task in 15 seconds, greatly enhancing diagnostic efficiency and reducing doctors' workload.

Usage Notes

The ASPECTS-281 atlas includes a series of two-dimensional atlases corresponding to the BGL and SGL across four age groups. We provide an automated pipeline for ASPECTS region mapping, making this atlas suitable for both rapid ASPECTS scoring in clinical practice as well as for relevant neuroscience research. The atlas is available in NIfTI format, allowing compatibility with various open-source tools such as ITK-SNAP and 3D Slicer.

Code availability

The complete codebase for constructing and mapping the ASPECTS-281, as well as the final atlas files of different age groups, are available in the GitHub repository (https://github.com/BravoSun/NCCT-atlas-for-ASPECTS-scoring). The atlas construction pipeline consists of two modules: the pre-processing module and the atlas generation module. The pre-processing module is used for symmetric alignment and brain tissue extraction. The atlas generation module is a bash script that utilizes the ANTs package with specific parameters for non-linear registration. Additionally, we also develop an ASPECTS atlas mapping pipeline, which enables the automated localization of the BGL and SGL as well as ASPECTS region mapping. All code is implemented in Python, and a trained ASPECTSLoc-Net is provided.

References

1. Kim, J. *et al*. Global stroke statistics 2019. international journal of stroke. *International Journal of Stroke* **15**, https://doi.org/10.1177/1747493020909545 (2020).
2. Murphy, S. & Werring, D. Stroke: Causes and clinical features. *Medicine (Abingdon)* **48**, https://doi.org/10.1016/j.mpmed.2020.06.002 (2020).
3. Wu, S. *et al*. Stroke in china: advances and challenges in epidemiology, prevention, and management. *Lancet Neurol.* **18** (2019).
4. Chinese Health Statistics Yearbook (Beijing Union Medical University Press, Beijing, 2019).
5. Feigin, V., Lawes, C., Bennett, D., Barker-Collo, S. & Parag, V. Worldwide stroke incidence and early case fatality reported in 56 population-based studies: a systematic review. *Lancet Neurol* **8**, https://doi.org/10.1016/S1474-4422(09)70025-0 (2009).
6. Wang, Y. *et al*. Chinese stroke association guidelines for clinical management of cerebrovascular disorders: executive summary and 2019 update of the management of high-risk population. *Stroke Vasc Neurol* **5**, https://doi.org/10.1136/svn-2020-000385 (2020).
7. Powers, W. *et al*. Guidelines for the early management of patients with acute ischemic stroke: 2019 update to the 2018 guidelines for the early management of acute ischemic stroke: A guideline for healthcare professionals from the american heart association/american stroke association. *Stroke* **50**, https://doi.org/10.1161/STR.0000000000000211 (2019).
8. Barber, P., Demchuk, A. & Zhang, A., Buchan, J. Validity and reliability of a quantitative computed tomography score in predicting outcome of hyperacute stroke before thrombolytic therapy. *Lancet North Am. Ed.* **255**, https://doi.org/10.1016/s0140-6736(00)02237-6 (2000).
9. Mullins, M., Lev, M., Schellingerhout, D., Koroshetz, W. & Gonzalez, R. Influence of availability of clinical history on detection of early stroke using unenhanced ct and diffusion-weighted mr imaging. *AJR Am. J. Roentgenol.* **179**, https://doi.org/10.2214/ajr.179.1.1790223 (2002).
10. Neuhaus, A. *et al*. Region-specific agreement in aspects estimation between neuroradiologists and e-aspects software. *Journal of Neurointerventional Surgery* **12**, https://doi.org/10.1136/neurintsurg-2019-015442 (2020).
11. Evans, A. *et al*. 3d statistical neuroanatomical models from 305 mri volumes. In *1993 IEEE Conference Record Nuclear Science Symposium and Medical Imaging Conference,* vol. 3, 1813–1817, https://doi.org/10.1109/NSSMIC.1993.373602 (1993).
12. Collins, D., Neelin, P., Peters, T. & Evans, A. Automatic 3d intersubject registration of mr volumetric data in standardized talairach space. *J. Comput. Assist. Tomogr.* **18** (1994).
13. Mazziotta, J., Toga, A., Evans, A., Fox, P. & Lancaster, J. A probabilistic atlas of the human brain: theory and rationale for its development. *Neuroimage* **2**, https://doi.org/10.1006/nimg.1995.1012 (1995).
14. Mazziotta, J. *et al*. A four-dimensional probabilistic atlas of the human brain. *J. Am. Med. Inform. Assoc.* **8**, https://doi.org/10.1136/jamia.2001.0080401 (2001).
15. Mazziotta, J. *et al*. A probabilistic atlas and reference system for the human brain: International consortium for brain mapping (icbm). *Philos. Trans. R. Soc. B-Biol. Sci.* **356**, https://doi.org/10.1098/rstb.2001.0915 (2001).
16. Shattuck, D. *et al*. Construction of a 3d probabilistic atlas of human cortical structures. *Neuroimage* **39**, https://doi.org/10.1016/j.neuroimage.2007.09.031 (2008).
17. Tang, Y. *et al*. The construction of a chinese mri brain atlas: A morphometric comparison study between chinese and caucasian cohorts. *Neuroimage* **51**, https://doi.org/10.1016/j.neuroimage.2010.01.111 (2010).
18. Liang, P. *et al*. Construction of brain atlases based on a multi-center mri dataset of 2020 chinese adults. *Sci. Rep.* **5**, https://doi.org/10.1038/srep18216 (2015).
19. Rorden, C., Bonilha, L., Fridriksson, J., Bender, B. & Karnath, H. Age-specific ct and mri templates for spatial normalization. *Neuroimage* **61**, https://doi.org/10.1016/j.neuroimage.2012.03.020 (2012).
20. Rajashekar, D. *et al*. High-resolution t2-flair and non-contrast ct brain atlas of the elderly. *Sci. Data* **7**, https://doi.org/10.1038/s41597-020-0379-9 (2020).

21. Schröder, J. & Thomalla, G. A critical review of alberta stroke program early ct score for evaluation of acute stroke imaging. *Front Neurol.* **7**, https://doi.org/10.3389/fneur.2016.00245 (2017).
22. Mallon, D. *et al.* Real-world evaluation of brainomix e-stroke software. *Stroke Vasc Neurol.* **svn-2023-002859**, https://doi.org/10.1136/svn-2023-002859 (2023).
23. Seyedsaadat, S. *et al.* Differential contribution of aspects regions to clinical outcome after thrombectomy for acute ischemic stroke. *Am. J. Neuroradiol.* **42**, https://doi.org/10.3174/ajnr.A7096 (2021).
24. Ni, H. *et al.* Asymmetry disentanglement network for interpretable acute ischemic stroke infarct segmentation in non-contrast ct scans. In *Medical Image Computing and Computer Assisted Intervention*, vol. 13438, 416–426, https://doi.org/10.1007/978-3-031-16452-1_40 (2022).
25. Jaderberg, M., Simonyan, K., Zisserman, A. & Kavukcuoglu, K. Spatial transformer networks. In *Advances in Neural Information Processing Systems 28*, vol. 2, 2017–2025 (2015).
26. Avants, B. B., Epstein, C. L., Grossman, M. & Gee, J. C. Symmetric diffeomorphic image registration with cross-correlation: Evaluating automated labeling of elderly and neurodegenerative brain. *Med. Image Anal.* **12**, https://doi.org/10.1016/j.media.2007.06.004 (2008).
27. Avants, B. *et al. Neuroimage* **54**, https://doi.org/10.1016/j.neuroimage.2010.09.025 (2011).
28. Sun, Q. *et al.* Age-specific aspects atlas of chinese subjects across different age groups for assessing acute ischemic stroke. *figshare* https://doi.org/10.6084/m9.figshare.26819290 (2024).
29. Liu, X. *et al. IEEE Transactions on Medical Imaging* **34**, https://doi.org/10.1109/TMI.2015.2448556 (2015).
30. Horchreiter, S. & Schmidhuber, J. Long short-term memory. *Neural Computation.* **9**, https://doi.org/10.1162/neco.1997.9.8.1735 (1997).
31. Yun, S. *et al.* Cutmix: Regularization strategy to train strong classifiers with localizable features (2019).

Acknowledgements

Author contributions

Qi Sun: Study design, image processing, data analysis, manuscript drafting and revising. Guan Wang: Visual inspection, ASPECTS region annotation and clinical evaluation. Jinzhu Yang: Research supervise and manuscript revising. Yimo Zhou: Data collection and screening, as well as ASPECTS region annotation. Yuliang Yuan, Yan Huang and Ziyu Fu: Assisting data analysis.

Competing interests

The authors declare no competing interests.

Additional information

Correspondence and requests for materials should be addressed to J.Y.

Reprints and permissions information is available at www.nature.com/reprints.

Publisher's note Springer Nature remains neutral with regard to jurisdictional claims in published maps and institutional affiliations.